Food Sci. Technol. Res., **7** (3), 183–190, 2001

Review

Advances in Transport Phenomena during Freeze-Drying of Food Materials: Fundamentals and Applications

Yasuyuki SAGARA

Department of Global Agricultural Sciences, Graduate School of Agricultural and Life Sciences, The University of Tokyo, Yayoi 1-1-1 Bunkyo-ku Tokyo 113-8657, Japan

Received August 3, 2001; Accepted August 16, 2001

Measurement method and values of thermal conductivity and permeability of water vapor were presented for the dried layer of food materials undergoing freeze-drying. Some structural models were developed for predicting the permeability of water vapor flowing through the dried layer. In a cellular food model, the resistance of a cell membrane to the molecular transfer of water vapor was determined from both value of permeability and microscopic observation of average diameter of cells. The model was considered to play an important role in predicting optimum heating program for the surface temperature of materials. A micro-slicer image processing system (MSIPS) has been developed for measuring the three-dimensional (3-D) structure and distribution of ice crystals formed in frozen food materials. The system has functions to reconstruct the 3-D image based on the image data of exposed cross sections obtained by multi-slicing of a frozen sample with the minimum thickness of 1 μm and to display the internal structure as well as an arbitrary cross section of the sample choosing observation angles. The effects of freezing conditions on the morphology and distribution of ice crystals were demonstrated quantitatively from the observations of raw beef stained by fluorescent indicator of muscle fibers. The scale-up procedures were described for optimizing the design and operation of industrial freeze-dryer to produce dried-egg soups.

Keywords: freeze-drying, transport phenomena, food, thermal conductivity, permeability of water vapor, ice crystal, scale up

Freeze-drying has had a great impact upon the production of dehydrated foods because of the superior quality of the product obtained and promises continued expansion of the numbers of applications. However, the process is only feasible if the cost of production can be lowered by optimum plant operations. Since the freeze-drying rate is limited by the rates of heat and mass transfer across a dried layer, the values of its thermal conductivity and permeability are indispensable to determine the drying rate. These values are mainly governed by the structure of the dried layer and then operating factors such as temperature and pressure. Since the structural nature of the dried layer is also affected by freezing operations, the relationships among the freezing condition, structure and transport properties of the dried layer are the fundamental information to design the optimum drying cycle and control the quality of final products.

This paper presents (1) the measurement method and values of transport properties for the dried layer of food materials, (2) the structural models for predicting the value of permeability, (3) a micro-slicer image processing system (MSIPS) for measuring the 3-D structure and distribution of ice crystals formed in frozen food materials and then (4) demonstrates an technical cooperation project between university and industry for optimizing the design and operation of industrial freeze-drier to produce dried-egg soups.

Theoretical Model

Model for transport properties analysis Figure 1 shows a uniformly-retreating-ice front (URIF) model to determine the transport properties for the dried layer of the material undergoing freeze-drying. Based on several assumptions, the equations of heat and mass fluxes were introduced to the dried layer for obtaining the equations to determine the values of thermal conductivity and permeability from drying data (Sagara & Hosokawa, 1982; Sagara *et al.*, 1982; Sagara, 1992).

Capillary structural model An approximate method was developed for predicting the structural parameters of the dried layer by assuming this layer to be a bundle of capillary tubes with the pore space having an equivalent pore radius, porosity and tortuosity factor (Sagara, 1986). The mass flux of water vapor flowing through the dried layer may be written as:

$$\dot{m} = -\frac{Km_w}{RT} grad\ p. \tag{1}$$

The expressions for the permeability coefficient of a single capillary tube are taken from Mellor and Lovett (1964);

$$K = \frac{\varepsilon}{\tau} D_k \Omega, \tag{2}$$

where,

$$\Omega = \underset{\text{(Poiseulle)}}{\frac{3\pi r}{64\lambda}} + \underset{\text{(Slip)}}{\frac{\pi}{4}\frac{2r/\lambda}{(1+2r/\lambda)}} + \underset{\text{(Knudsen)}}{\frac{1}{1+2r/\lambda}}. \tag{3}$$

In this equation the value of Ω expresses the total of separate contributions due to Poiseulle's flow, slip flow and Knudsen's flow. From the above relation, Ω can be expressed as a function of r and T/p since λ is defined in terms of a ratio of absolute temperature to pressure. The mean free path of a water-vapor mole-

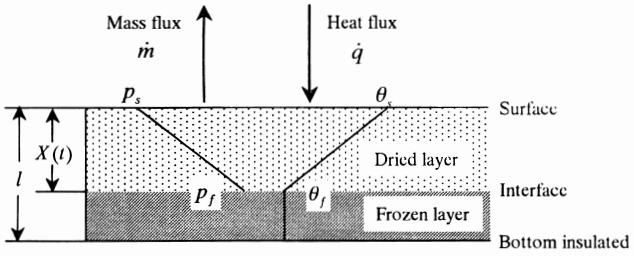

Fig. 1. Freeze-drying model to determine transport properties.

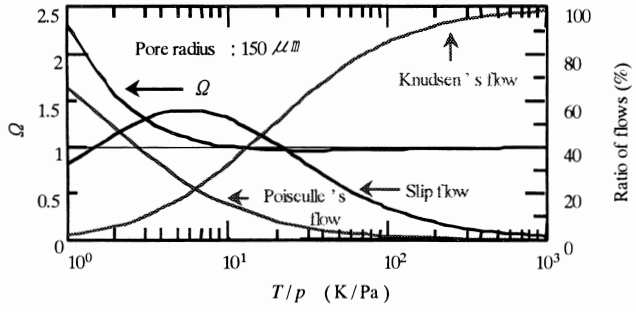

Fig. 2. Variation of Ω with T/p and the ratios of flows contribute to Ω.

cule λ is given by

$$\lambda = \frac{\kappa T}{\sqrt{2}\pi\sigma_w^2 p}. \quad (4)$$

The Knudsen diffusivity was defined in terms of the pore radius and the average molecular velocity as follows:

$$D_k = \frac{2}{3}\bar{v}r, \quad \text{where} \quad \bar{v} = \left(\frac{8RT}{\pi M_w}\right)^{\frac{1}{2}}. \quad (5)$$

Since the pore radius of several freeze-dried foods is in the range of 10–300 μm, the effects of T/p as well as each flow on Ω were investigated and then illustrated as shown in Fig. 2, assuming the equivalent pore radius of 150 μm. The curve of Ω has been found to approach unity with an increase in the ratio of Knudsen's flow to the total. Since in usual operating conditions the ratio T/p is assessed to be in the range of 4 to 10, the function Ω can be approximated to be unity. Then the pore structural ratio r/τ is estimated from equations (2) and (5). Combining these equations, one get

$$K = A\sqrt{T}, \quad \text{where} \quad A = \frac{r}{\tau}\varepsilon\frac{2}{3}\left(\frac{8R}{\pi M_w}\right)^{\frac{1}{2}}. \quad (6)$$

As indicated in equation (6) the slope of a curve fitted to the plot of permeability against $\sqrt{T}$ provides the constant value A and thus the ratio r/τ can be determined.

After obtaining the values of structural parameters, they were applied to an equation presented by Mellor and Lovett (1964), which was derived on the basis of collision theory for the permeability in term of the mean free path, giving

$$K = \frac{\varepsilon}{\tau}D_k\left[\left\{\frac{3}{32k'}\frac{2r}{\lambda} + \delta_1\right\}\cdot(1 - e^{-2r/\lambda}) + e^{-2r/\lambda}\right]. \quad (7)$$

As shown in the following section the equation (7) has been found to fit the experimental results for raw beef and coffee solutions over the wide pressure ranges.

Cellular structural model Values of the permeability for sliced apples calculated by the capillary model were found to be more than 10 times greater than those of measured. As an alternative a cellular structural model has been proposed as shown in Fig. 3 (Araki *et al.*, 2001). In the model, a cell is assumed to be a cylindrical geometry having an equivalent diameter d_c and l_c in length, respectively. The n layers of the cell are stacked parallel to the direction of water vapor transfer within the distance $X(t)$ between the surface and sublimation front of the sample. By utilizing the analogy of electrical circuit, the resistance against the flow of water vapor R_n was determined as the summation of an equivalent resistance R_s of each membrane. These two structural parameters were then introduced to modify the equation (2) for single capillary tube as follows;

$$K = \left(\frac{\varepsilon}{\tau}D_k\Omega\right)/R_n, \quad (8)$$

$$R_n = (n+1)R_s; R_0 = 1. \quad (9)$$

In the modified model the tortuosity factor τ was assumed to be unity because of the assumption of cells connected in series, and also the value of Ω can be assumed to be unity under our experimental conditions.

As above-mentioned, the parameter R_s can be calculated by carrying out once-time freeze-drying experiment and the microscopic observation of average diameter of cells, and thus the value of permeability could be determined for sliced samples. However, the availability of the model depends on some factors such as the average diameter of cells, accuracy of temperature measurement as well as control at the sample surface and geometrical stability of sublimation front that is foreseen to be lost by thermal edge effect during the later period of sublimation dehydration. To avoid these problems the average diameter of cells should be measured in the direction of mass or water-vapor transport, and the model is recommended to be applied during the period until the sublimation front reaches about 60% of sample thickness (Sagara, 2001).

The proposed model can be applied to other cellular food materials, and a predicted value is useful to calculate the mass transfer rate across the dried layer, and finally, it can be used to design optimum plant operations, or heating program for the surface of material whose drying rate is limited by mass transfer rate.

Micro-slicer Image Processing System

A novel technique has been developed for measuring the

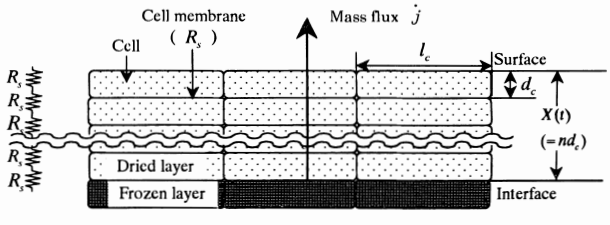

Fig. 3. Structural model for cellular food materials.

three-dimensional (3-D) structure and distribution of ice crystals formed in frozen foods and biological materials by using a Micro-Slicer Image Processing System (MSIPS). The system has functions to reconstruct the 3-D image based on the image data of exposed cross-sections obtained by multi-slicing of a frozen sample and to display the internal structure as well as an arbitrary cross-section of the sample choosing observation angles. The size and distribution of ice crystals can be determined from the 2-dimensional quantitative information such as the periphery and area of the crystals. The effects of freezing conditions on the morphology and distribution of ice crystals were demonstrated quantitatively from the observations of raw beef stained by fluorescent indicator.

Block diagram of MSIPS was shown in Fig. 4. The system is composed of a multi-slicing section to prepare the cross-sectional images of sample, observation unit, image recorder, controller and image processor or workstation. A personal computer is used to control both cross-sectioning machine and laser videodisk recorder. After the slicing operation, the 3-D sample image is reconstructed based on the image data of exposed cross-sections obtained by multi-slicing of a frozen sample with the minimum thickness of 1 μm and display the internal structure as well as an arbitrary cross-section of the sample choosing observation angles.

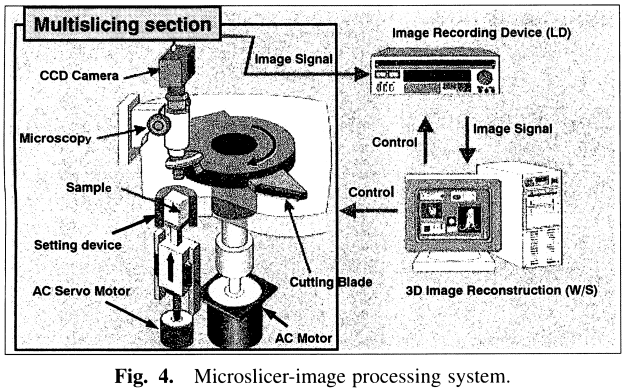

Fig. 4. Microslicer-image processing system.

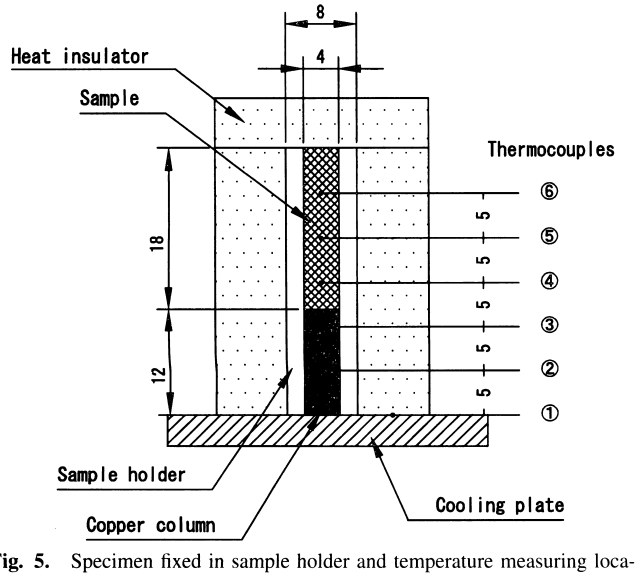

Fig. 5. Specimen fixed in sample holder and temperature measuring locations.

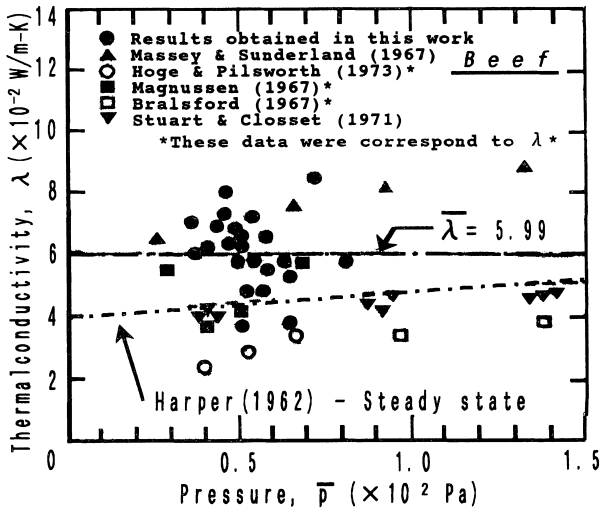

Fig. 6. Thermal conductivity vs. pressure for raw beef.

Fixing, freezing and slicing methods of the specimen Figure 5 shows the specimen embedded and fixed on a copper column with OCT (Optical Cutting Temperature) compound in a sample holder. The sample holder is a cylindrical paraffin vessel of 4 mm in inside diameter and 20 mm in height. For accomplishing one-dimensional freezing of the sample, an insulation material was placed around the side of the sample holder. The copper column located at lower part of the holder was used to determine the heat flux density during freezing. The temperature of copper cooling plate can be controlled at a constant temperature ranging from 0 to –150°C. After freezing, the fixed specimen was sliced together with the holder at the revolution rate of 60 rpm with the minimum thickness of 1 μm. The 3-D image of internal structure was reconstructed utilizing the 2-dimensional picture images. The size and distribution of ice crystals can be determined from the 2-dimensional quantitative information such as the periphery and area of the crystals.

Results and Discussion

Transport properties of raw beef The relationship between thermal conductivity and the pressure of the dried layer is shown in Fig. 6. Thermal conductivity λ* plotted in this figure is determined by neglecting the heat absorbed by water vapor flowing through the dried layer. Using a steady state method, Harper (1962) and Harper and El Sahrigi (1964) measured the thermal conductivities of freeze-dried beef, peach, apple and other materials with air or other high-conductivity gases surrounding the sample over a pressure range of 0.67 Pa to atmospheric. They concluded that the experimental data could be adequately correlated by an empirical equation based on concepts of unit cells involving combinations of series and parallel arrangements of the individual solid and gas phases. Since no data are given for beef in the presence of water vapor, a curve in Fig. 6 was calculated by applying the recommended values for air-filled beef to the empirical equation. However, there are some indications that the empirical equation does not accurately describe the thermal conductivity of freeze-dried beef when the surrounding gas is water

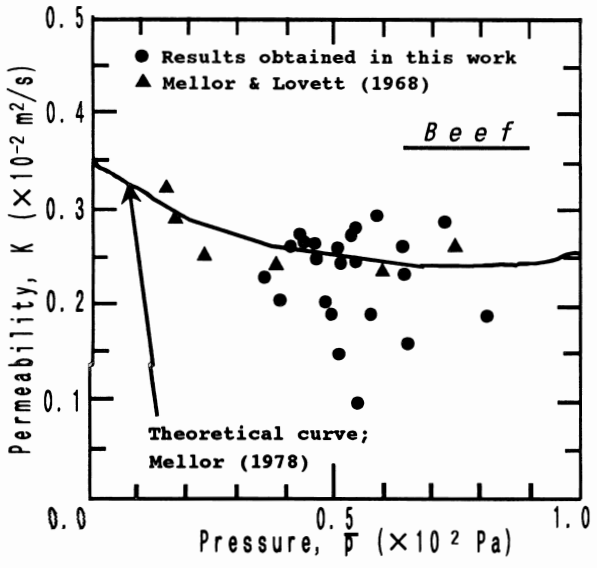

Fig. 7. Permeabilities vs. pressure for raw beef.

vapor. Bralsford (1967) and Hoge and Pilsworth (1973) indicated that their results for freeze-dried beef surrounded by water vapor were significantly different from those obtained with non-condensing gases and the values lay increasingly far above those for air. Triebes and King (1966) also reported the same behavior for freeze-dried cooked turkey meat. Our own data were found to be greater than those would be predicted for air-filled beef and appeared to confirm in this respect.

Although the effect of pressure on thermal conductivity was not recognized in our pressure range, it was considered that the conductivity essentially had a tendency to increase as the pressure increase. It is well known that the thermal conductivities of porous materials, when plotted vs. the logarithm of the pressure of the surrounding gas, provides characteristic sigmoid curves, indicating both lower and higher constant values in the low-pressure region below about 10 Pa and high-pressure above about 15 kPa, respectively. The lower constant value corresponds to the thermal conductivity of the solid phase and the higher to the apparent thermal conductivity of gas-filled solid matrix. The data plotted in Fig. 6 all fell in intermediate pressure region in which λ should increase with an increase in pressure. As shown in these results the contribution of gas phase confined in a solid matrix to the heat conduction process should be dependent upon the pressure level. The kinetic theory (Kennard, 1938) predicts that the gas thermal conductivity is independent of pressure as long as the mean free path is small compared with the sizes of void space in the matrix; as a consequence, the apparent thermal conductivity of the gas-filled solid matrix is independent of pressure. As the pressure is reduced, with the mean free path becoming comparable to and greater than the pore spacing, the gas thermal conductivity and thus the apparent conductivity of the matrix should begin to decrease continuously. At very low pressures, the gas provides a negative contribution to the total heat conduction, and thus a lower asymptotic conductivity of the solid matrix should be reached.

Plots of permeability vs. pressure for raw beef are shown in Fig. 7. The values of K were in good agreement with Mellor's theoretical curve based on a collision theory (Mellor & Lovett, 1964) and also their experimental data using completely freeze-dried samples under steady-state conditions. Table 1 shows the numerical values of the constant applied to the equation (7). As discussed by Mellor (1978), the theoretical curve demonstrated that the flow condition of water vapor transformed from Knudsen's to slip flows as the pressure increased.

Coffee solution Figure 8 shows the relationship between thermal conductivity and the porosity of the dried layer for coffee solutions. The results showed clearly that the thermal conductivity was markedly affected by solute concentration or the porosity of the dried layer. Porosity was assessed from cumulative composition using the value of 0.625 for the specific volume of pure coffee soluble. A linear relationship between thermal conductivity and porosity was obtained and the equation for a regression line fitted to all of the data was also presented in Fig. 8.

Figure 9 shows the relationship between permeability and porosity for coffee solutions at various temperatures of the dried layer. The permeability was found to depend mainly on the solute concentration or porosity of the dried layer and then other operating factors such as temperature or pressure. For example, the permeability for all samples of 40% in concentration (τ=0.7) were found to increase with an increase in the temperature of the dried layer. As is obvious from the kinetic theory of an ideal gas, the mean translational kinetic energy of a gas molecule is proportional to the absolute temperature. In accordance with this inter-

Table 1. Numerical values of the constant used to calculate permeability of beef sample by equation (7).

Constants	Numerical values used	Origin
r	58×10^{-6}, m	Mellor (1978)
k'	2.5, –	Mellor and Lovert (1964)
t	4.2, –	Mellor (1978)
δ_1	$3\pi/16$, –	Mellor and Lovert (1964)
σ	4.6×10^{-10}, m	Kennard (1938)
ε	0.64, –	Harper (1962)

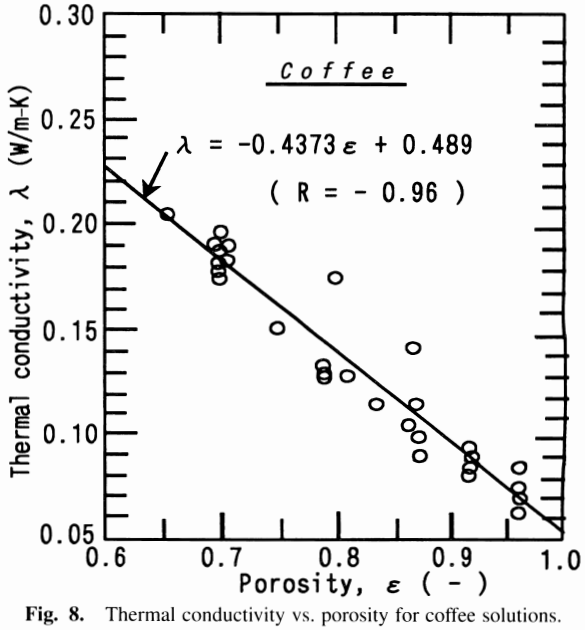

Fig. 8. Thermal conductivity vs. porosity for coffee solutions.

pretation the heat transfer from solid matrix to the molecules of water vapor is considered to accelerate their flow rate, providing the greater value of permeability. However, no theoretical investigation has been presented on heat transfer by both intermolecular and wall collisions for condensable gas such as water vapor. Although the pressure dependence of permeability was not definitely recognized in our pressure range, it has been demonstrated that the permeability increases as the pressure increase as indicated by freeze-dried beef samples. These behaviors were in good agreement with theoretical investigations based on the collision theory (Sagara, 1986) and also with experimental results obtained for concentrated tomato and sugar cane juices (Mellor, 1978).

As shown in Table 2 the equivalent pore radius r was predicted from the capillary model in the concentration range from 6.2 to 40.4%. The curve of K_{max} in Fig. 9 was calculated from the maximum values of temperature (26°C) as well as pressure (65 Pa), applying structural parameters obtained from equation (7). The calculation method of K_{min} follows the same procedure (–5°C, 25 Pa) as for K_{max}. As these curves demonstrate a similar porosity-dependent behavior of experimental plots, the assumptions made in this model appeared to be essentially reasonable (Sagara, 1986).

Apple Table 3 shows the values of the thermal conductivity and permeability for several food materials obtained by the URIF model. In this table the values of thermal conductivity for sliced and mashed apples were also presented. These data can be adequately calculated by the empirical equation presented by Harper (1962), and the thermal conductivity essentially had a tendency to increase as the pressure increased as indicated by raw beef samples. However, these absolute values were relatively larger than the empirical curve because in this study the "effective" value of thermal conductivity were measured under the existing conditions of temperature and pressure gradients across the dried layer of the sample undergoing freeze-drying.

Both resistance values of R_n and R_s in the cellular structural model were calculated for sliced apples by using measured values of permeability. The values of R_n were in the range of 42.5 to 96.2, while those of R_s were 2.9 to 7.3, and the average for them were determined to be 71.4 and 4.41, respectively. The mean values obtained for a sliced apple were used to predict the intrinsic permeability of apple flesh, and the predicted value was recognized to agree well with all measured permeability data under various drying conditions.

Effect of freezing rate on transport properties Figure 10 shows the freezing curves for mashed apple samples. The changes in temperature at the center during freezing could be regarded as an index of the freezing rate. Based on these indexes the mashed samples were classified into the group A and B. The

Table 2. Variation of pore radius with porosity for the dried layer of coffee solutions.

Pore radius	Porosity				
	0.7	0.8	0.86	0.92	0.96
r; Eq. (2)	59.4	70	70.9	95.4	117.5
r'; Eq. (7)	76.5	88.1	89.6	122.4	149.9
Δr; (%)	28.8	25.9	26.3	28.3	27.6

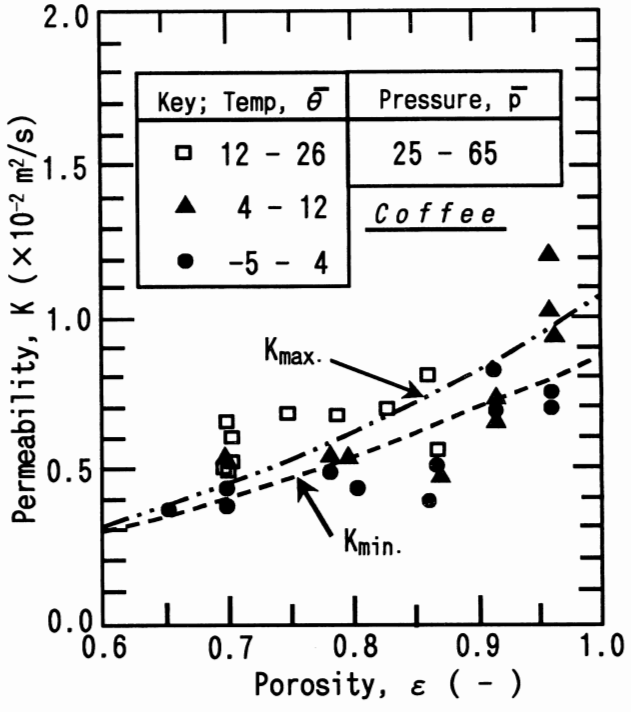

Fig. 9. Permeability vs. porosity for coffee solutions.

Table 3. Thermal conductivity and permeability for several food materials.

Material	Sample surface Temperature (°C)	Pressure in the chamber (Pa)	Temperature[a] (°C)	Pressure[a] (Pa)	Thermal conductivity (W/m·K)	Permeability (×10⁻²m²/s)	Reference
	θ_s	p_s	$\bar{\theta}$	$\bar{p}$	λ	K	
Sliced apple	−10–10	20–30	−17.7–−3.4	38.4–80.0	0.056–0.123	0.063–0.120	Araki *et al.* (1998)
Mashed apple (A)[b]	0–40	20–30	−13.6–8.5	33.5–46.2	0.11–0.13	0.40–0.50	Araki *et al.* (1998)
Mashed apple (B)[b]	10–70	20–30	−11.8–19.7	23.7–29.0	0.068–0.073	1.3–1.6	Araki *et al.* (1998)
Beef	30–100	7–30	3.0–40.8	38.2–78.5	0.036–0.084	0.090–0.405	Sagara *et al.* (1982)
Minced beef	40	2.7–13.3	7.3–10.3	—	0.050–0.069	0.13–0.24	Widodo and Tambunan (1966)
Coffee solution (6–30%)[c]	20–53	10–95	−5.3–14.8	—	0.062–0.172	0.340–1.220	Sagara and Hosokawa (1982)
Coffee solution (29–45%)[c]	−7–71	7–12	−14.1–26.1	47.1–66.8	0.153–0.277	0.213–0.649	Sagara and Ichiba (1994)
Coffee solution (10–36%)[c]	60	22–34	12.9–20.2	24.9–64.9	0.063–0.144	0.508–4.235	Ichiba (1994)
Shrimp	30–50	7–133	4.2–21.2	53.6–263	0.038–0.086	0.031–0.120	Wenur (1997)

[a]Average value for the dried layer, [b](A) Papid freezing and (B) Slow freezing, [c]Coffee solute concentration.

freezing rate of the group A was relatively larger than the group B. In order to obtain the quantitative index, the period between two inflection points was defined as the ice-crystallization time, based on the primary differential values of these curves.

Figure 11 shows a linear relationship between permeability and ice crystallization time for mashed samples. This behavior are attributed to the larger ice crystals formed in the sample as the freezing rate decreased. Hence, the effects of the freezing rate on transport properties, especially on the permeability, were found to be critical for the mashed cellular food materials. In liquid food systems the porosity of the dried layer is governed by the solid content or concentration, and thus the porosity mainly affects the thermal conductivity of the dried layer as shown in Fig. 8. In addition to concentration the permeability is influenced significantly by freezing manner, because the capillary type ice columns is formed by ice crystals along with the direction of heat flow during freezing (Sagara, 1986), and the smaller size of ice crystals is formed with an increase in freezing rate. Consequently, the morphology of capillary type void as well as grain orientation and the pore size of the dried layer are arranged during a freezing process, and thus the transport properties of the dried layer is decisively governed by the structure fixed during freezing.

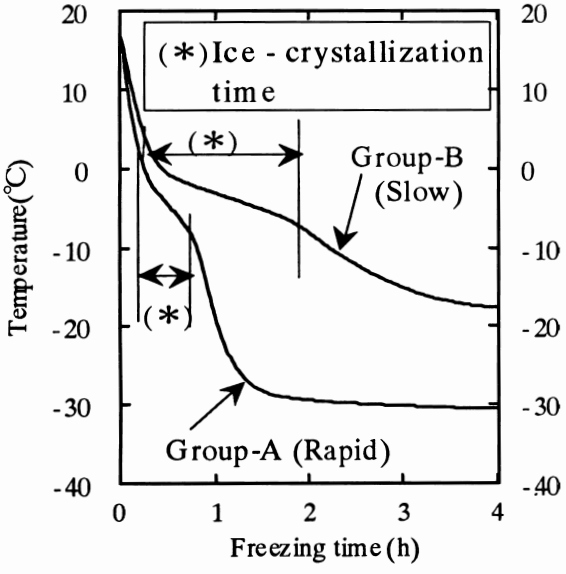

Fig. 10. Freezing curve for mashed apples.

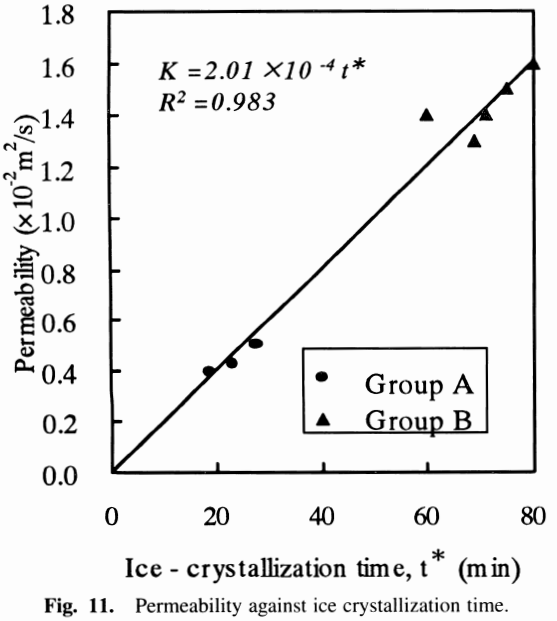

Fig. 11. Permeability against ice crystallization time.

From these results, it would be suggested for liquid materials that under the constant solid concentration the material should be frozen in a manner to form straight ice columns whose orientation is parallel to that of heat transport during drying and also make larger ice crystals by employing the slower freezing rate. If the higher permeability coefficient could be obtained by controlling freezing method, the drying rate would be limited by heat transfer rate across the dried layer. Under this condition the surface temperature of the dried layer is allowed to increase within a certain range that is decided from the viewpoint of quality control for final products.

Structure and distribution of ice crystals Figure 12 shows a typical cross-sectional image obtained from the lower parts of the specimen frozen at the bottom surface temperature of −120°C. The images showed clearly ice crystals and muscle fibers, indicating the intercellular networks of ice crystals of 20–30 μm in diameter and also spherical crystals 10–20 μm at inner space of cells. These cross-sectional images demonstrated that the variation in morphology as well as configurations of ice crystals reflected the difference in heat transfer rates during freezing processes (Sagara, 2001).

Figure 13 shows the 3-D images of the specimens frozen at −120°C. As shown in these images, the MSIPS was demonstrated to be useful to observe the growth of inter- and extracellular ice columns. These images showed that the ice crystals formed the columns that grew towards the interior of the meat in the opposite direction to heat flux, starting at the bottom or cooling surface of specimen. The ice column was developed mainly in intercellular spaces at surface portion, causing the large distortion of cell as shown in cross sectional image. These images were also found to support the well-known hypothesis that the site of ice crystal growth was transferred gradually from extra- to intracellular location as the freezing rate increased, forming smaller spherical ice crystals and increasing their population within the

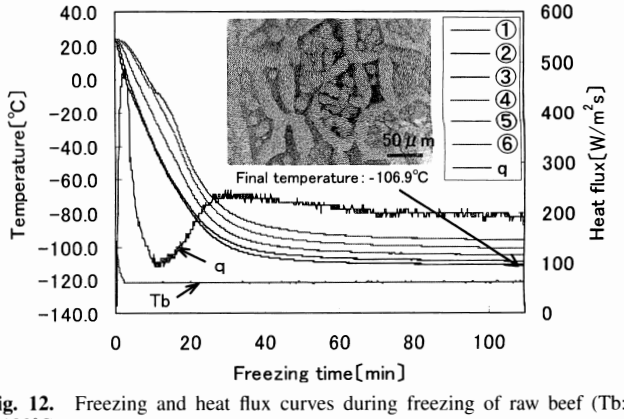

Fig. 12. Freezing and heat flux curves during freezing of raw beef (Tb: −120°C).

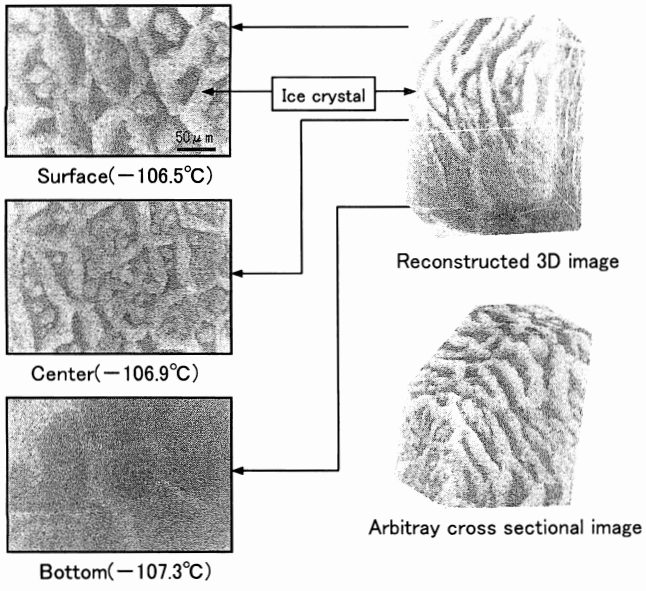

Fig. 13. Reconstructed 3D images of frozen beef 1 mm in thickness.

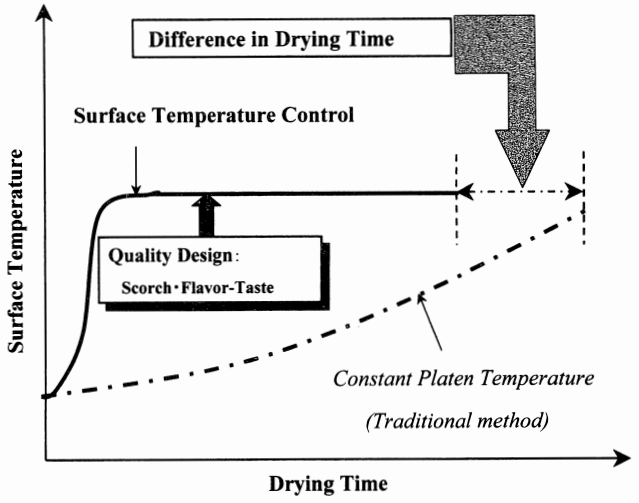

Fig. 14. Shortening of drying time by surface temperature control of material.

cell. The growth of ice columns appeared to be restricted by the intrinsic structure of muscle fibers. Furthermore, the continuity of columns had a tendency to be lost at lower portion because of smaller crystal size formed.

The continuity of ice column appeared to be an important factor, which affects not only the texture of frozen beef after thawing as well as cooking but also the permeability of water vapor flowing through the dried layer during freeze-drying. As described here, the three-dimensional images of a frozen beef tissue were recognized to be useful for investigating the mechanisms in the growing process of ice column. These results indicated that the proposed method provided a new tool to investigate the effects of freezing conditions on the structure and then transport properties for the dried layer of the materials undergoing freeze-drying.

Scale up to industrial freeze-drier for producing egg soups A technical cooperation project has been carried out between university and industries for optimizing the design and operation of industrial freeze-dryer to produce dried-egg soups. The batch-type freeze dryers in industrial scale have been usually operated at a constant temperature of platens. The temperature of platen has been decided empirically by considering the heating condition for performing high production efficiency without deterioration in final product. After designing the recipe of product, some food companies are entrusting another processor having a freeze-drying plant with a production. Since the processors have to receive the raw materials of various brands, they are required to control their plant under a safe condition that generally applicable to all received materials. To increase the productivity of the plant, the specified control program should be applied for each product. However, it is now difficult to accomplish this manner, because the useful information is limited in number to design a controlling program. Then almost of the plant for food materials is operated under a constant temperature of heating platens even though their drying rates are usually limited by heat transfer rate. For egg soup mixture, a drying cycle required more than 24 h by this traditional heating method.

Figure 14 shows a new heating program in which the sample surface is maintained at a constant temperature immediately after heating start. This accomplished by using the program control method for the platen. The constant temperature at surface of material was determined from a standpoint of quality design for final product. The general factors, which should be considered for designing quality, are related mainly to taste and flavor retention. However, in this control the change in surface color by scorching becomes most important factor. We found that the drying time has been shortened by more than 4 h by applying this program to egg soup mixture. Then a manufacturing company participated to the project in order to realize this method in their plant. In designing the plant, the manufacturer selected the material for the platen that could bear against the high temperature of heating medium circulating in it and modified their traditional plant. The new freeze-dryer was introduced to the processing plant of a food company and started successfully their production in 1999. The production cycle including preparation and packaging processes was shortened within 24 h, saving the costs of energy and labor without the shift of working time. The patent for egg soup production was submitted from the project and opened now.

Conclusion

To optimize freeze-drying cycle both development of new technologies and implements related to the design as well as operation of dryers are desirable based on fundamental information existing among the freezing condition, structure as well as transport properties of the dried layer and quality of final products. Especially, the information becomes more important for drying solution systems because their structure is controllable artificially. If we could obtain fundamental knowledge, the computer simulation model including a series of freezing and freeze-drying processes would provide a strong tool to investigate the optimum design and control methods. As shown in this paper, the technical cooperation between university and private company will be a key factor in further development of industrial freeze-drying plants.

Nomenclatures

A	constant
D_k	Knudsen diffusion coefficient, m^2/s
d	diameter, m
j	water-vapor flux, kg/(m^2-s)
K	permeability, m^2/s
k'	structural constant, -
l	length, m
$\dot{m}$	mass flux density, kg/(m^2-s)
M	molecular weight, kg/mol
n	number of cells
p	pressure, Pa
$\dot{q}$	heat flux density, J/(m^2-s)
R	gas constant, J/(mol-K)
R_n	resistance against the water vapor, -
R_s	equivalent resistance of each membrane, -
r	equivalent pore radius, m
T	absolute temperature, K
t	time, s
$\bar{v}$	average molecular velocity, m/s
$X(t)$	position of the sublimation front, -

⟨Greek letters⟩

δ_1	roughness factor of pore, -
ε	porosity, -
θ	temperature, °C
κ	Boltzmann constant
λ	thermal conductivity, W/(m-K)
	mean free path of the gas molecules, m in eqs. (3), (4), and (7)
σ	diameter of a molecule, m
τ	tortuosity factor, -
Ω	total of separate contributions due to Poiseulle's flow, slip flow and Knudsen's flow, -

⟨Subscripts⟩

c	cell
f	sublimation front
s	surface
w	water vapor

References

Araki, T., Sagara,Y., Tambunan, A.H. and Kamaruddin, A. (1998). Measurement of transport properties for the dried layer of several food materials undergoing freeze-drying. *Bul. Keteknikan Pertanian.*, **12**, 18–31.

Araki, T., Sagara, Y., Kamaruddin, A. Tambunan, A.H. (2001). Transport properties of cellular food materials undergoing freeze-drying. *Drying Technol.*, **19**, 297–312.

Bralsford, R. (1967). Freeze drying of beef, 1. Theoretical freeze-drying rates of beef, 2. A calorimetric method for comparing theoretical and actual drying rates. *J. Food Technol.*. **2**, 339–353.

Harper, J.C. (1962). Transport properties of gases in porous media at reduced pressures with reference to freeze-drying. *AIChE J.*, **8**, 298–302.

Harper, J. C. and El Sahrigi, A.F., (1964). Thermal conductivities of gas-filled porous solids. *I & EC Fundam.*, **3**, 318–324.

Hoge, H.J. and Pilsworth Jr, M.N. (1973). Freeze drying of beef: Theory and experiment. *J. Food Sci.*, **38**, 841–847.

Ichiba, J. (1994). The Effect of Freezing rate on drying characteristics of granular food materials: Change in the structure and transport properties. MD's Thesis, The University of Tokyo, 60–62.

Kennard, E. H. (1938). "Kinetic Theory of Gases." P. 149, McGrow-Hill.

Mellor, J.D. and Lovett, D.A. (1964). Flow of gases through channels with reference to porous material. *Vacuum*, **18**, 625.

Mellor, J.D. (1978). "Fundamentals of Freeze-Drying." Academic Press, London, pp. 94–128.

Sagara, Y., Kameoka, T. and Hosokawa, A. (1982). Measurement of thermal conductivity and permeability of the dried layer during freeze drying of beef. *J. Soc. Agric. Mach., Jpn*, **44**, 477–487.

Sagara, Y. and Hosokawa, A. (1982). Dry layer transport properties and freeze-drying characteristics of coffee solutions. Proc. Third Int. Drying Symposium (IDS'82), Birmingham, 487–496.

Sagara, Y. (1986). Transport Properties Measurement of Food Sample Undergoing Sublimation Dehydration. Proc. Fifth Int. Drying Symposium (IDS '86), MIT, Cambridge, 1, pp. 413–421.

Sagara, Y. (1992). Automatic Measurement System for Transport Properties of Food Samples Undergoing Sublimation Dehydration. Advances in Food Engineering. CRC Press, pp. 111–124.

Sagara, Y. and Ichiba, J. (1994). Measurement of transport properties for the dried layer of coffee solution undergoing freeze drying. *Drying Technol.*, **12**, 1081–1103.

Sagara, Y. (2001). Structural models related to transport properties for the dried layer of food materials undergoing freeze-drying. *Drying Technol.*, **19**, 281–296.

Triebes, T.A. and King, C.J. (1966). Factors influencing the rate of heat conduction in freeze drying. *I&EC Process Design Dev.*, **5**, 430–435.